Nanoscale

ROYAL SOCIETY OF CHEMISTRY

PAPER

View Article Online
View Journal | View Issue

Check for updates

Cite this: *Nanoscale*, 2023, **15**, 1076

Ultrasensitive detection of SARS-CoV-2 spike protein by graphene field-effect transistors†

Alessandro Silvestri, ‡[a] Julian Zayas-Arrabal, §‡[a] Mariano Vera-Hidalgo,[a] Desire Di Silvio,[a] Cecilia Wetzl, [a,b] Marta Martinez-Moro,[a] Amaia Zurutuza,[c] Elias Torres,[c] Alba Centeno,[c] Arantxa Maestre,[c] Juan Manuel Gómez,[c] María Arrastua,[c] Marta Elicegui,[c] Nerea Ontoso,[c] Maurizio Prato, *[a,d,e] Ivan Coluzza*[f,e] and Alejandro Criado *[a,g]

Received 16th September 2022,
Accepted 16th December 2022

DOI: 10.1039/d2nr05103f

rsc.li/nanoscale

COVID-19, caused by the severe acute respiratory syndrome-coronavirus 2 (SARS-CoV-2), originated a global health crisis, causing over 2 million casualties and altering human daily life all over the world. This pandemic emergency revealed the limitations of current diagnostic tests, highlighting the urgency to develop faster, more precise and sensitive sensors. Graphene field effect transistors (GFET) are analytical platforms that enclose all these requirements. However, the design of a sensitive and robust GFET is not a straightforward objective. In this work, we report a GFET array biosensor for the detection of SARS-CoV-2 spike protein using the human membrane protein involved in the virus internalisation: angiotensin-converting enzyme 2 (ACE2). By finely controlling the graphene functionalisation, by tuning the Debye length, and by deeply characterising the ACE2-spike protein interactions, we have been able to detect the target protein with an extremely low limit of detection (2.94 aM). This work set the basis for a new class of analytical platforms, based on human membrane proteins, with the potential to detect a broad variety of pathogens, even before their isolation, being a powerful tool in the fight against future pandemics.

Introduction

The recent COVID-19 pandemic emergency has demonstrated how our society is exposed to infectious diseases. The current state-of-the-art technologies for the detection of pathogens cannot achieve rapidity, selectivity, sensibility, and reliability at once.[1] For instance, polymerase chain reaction (PCR) is a very sensitive and robust method, and the primary means of diagnosis for emerging pathogens.[2] However, it takes a long time to amplify the virus DNA and the process requires bulky instrumentation. On the other side, lateral flow antigenic tests are fast, cheap, portable, and easy to perform, but are frequently affected by poor clinical or diagnostic sensitivity.[1] For these reasons, these methods, which have been frequently used in the fight against several infectious diseases, fell short in times of high demand for fast and accurate population screening.

To prevent future global pandemics, it is key to develop new platforms able to rapidly detect viruses and test their infectivity.[3] As in the case of COVID-19, future potential threats could arise from unknown viruses. Therefore, effective sensors should be able to detect such viruses even before their isolation and identification. The state-of-the-art analytical devices, based on monoclonal antibodies (mAbs), are unable to accomplish this task.

A strategy to create sensors able to detect a broad variety of viruses is to employ the human membrane proteins involved in the internalisation of target pathogens. In this sense, a good candidate is Angiotensin-converting enzyme 2 (ACE2), an enzyme expressed on the membrane of human cells of the intestine, kidney, testis, gallbladder, and heart. This protein can interact with the spike glycoprotein of coronaviruses serving as an entry point for pathogens.[4,5]

[a]*Center for Cooperative Research in Biomaterials (CIC biomaGUNE), Basque Research and Technology Alliance (BRTA), Paseo de Miramon 194, 20014 Donostia-San Sebastián, Spain. E-mail: mprato@cicbiomagune.es*
[b]*University of the Basque Country UPV-EHU, 20018 Donostia-San Sebastián, Spain*
[c]*Graphenea Semiconductor SLU., Paseo Mikeletegi 83, 20009 San Sebastián, Spain*
[d]*Department of Chemical and Pharmaceutical Sciences, University of Trieste, Via L. Giorgieri 1, 3412 7 Trieste, Italy*
[e]*Ikerbasque, Basque Foundation for Science, 48013 Bilbao, Spain*
[f]*BCMaterials, Basque Center for Materials, Applications and Nanostructures, Bld. Martina Casiano, UPV/EHU Science Park, Barrio Sarriena s/n, 48940 Leioa, Spain. E-mail: ivan.coluzza@bcmaterials.net*
[g]*Universidade da Coruña, CICA – Centro Interdisciplinar de Química e Bioloxía, Rúa as Carballeiras, 15071 A Coruña, Spain. E-mail: a.criado@udc.es*

†Electronic supplementary information (ESI) available. See DOI: **https://doi.org/10.1039/d2nr05103f**

‡These authors contributed equally to the work.

§Current address: Departmento de Pediatría, Universidad del País Vasco UPV/EHU, 20014 San Sebastian, Spain.

The use of ACE2 as a receptor, instead of monoclonal antibodies, provides a series of advantages. In first instance, the expression of a monoclonal antibody with elevated selectivity for a specific virus requires the isolation of the virus.[6] Instead, by using ACE2, it will be possible to detect selectively the infective viruses whose internalization in cells is mediated through this human receptor. Finally, by using ACE2 as a receptor the efficacy of the biosensor will not be affected by virus mutations. SARS-CoV-2 has been a clear example of how fast viruses can mutate, producing several variants in the span of time of 2 years. When a mutation induces alterations of the topography and composition of the pathogen surface, antibody-based biosensors are likely to lose their efficacy.[7]

In this work, we combined the ability of ACE2 to interact with the spike protein of coronaviruses with the elevated sensitivity provided by graphene field effect transistors (GFETs), developing a platform with the potential to detect pathogenic viruses. GFETs are emerging as highly sensitive bioanalytical sensors, whose responsive electrical conductance is used to perform quantitative analysis of biologically relevant molecules such as DNA, proteins, ions, and small molecules among others.[8,9]

Several platforms for the detection of viruses have already been published in the literature, recently addressing the detection of SARS-CoV-2.[10] Owing to the elevated sensibility, miniaturisation capability, rapid detection ability, and industrial scalability, GFETs were widely investigated for this aim.[8,9] The efficient detection of SARS-CoV-2 with GFETs has been proved in several recent works. The first to report it were Seo *et al.* in 2020, using a GFET transistor functionalised with mAbs for the detection of the whole virus.[2] Xu *et al.* have recently reported an aptasensor based on GFETs to detect the spike protein and the whole SARS-CoV-2 virus with a LOD of 3 fM and $10–10^2$ copies per μL, respectively.[2] In 2021, Kong *et al.* functionalised GFETs with Y-shaped DNA dual probes to target ORF1ab and N genes of SARS-CoV-2 nucleic acid.[11] Park *et al.* reported a FET based on crumpled graphene that, when combined with reverse transcriptase loop-mediated isothermal amplification (RT-LAMP), allows the detection of SS-DNA RT-LAMP primers of SARS-CoV-2.[12] However, in both these cases, the previous amplification of the virus DNA is required. An alternative approach using GFET transistor was proposed by Kang *et al.*, who functionalised graphene with the spike protein of coronavirus for the sensitive detection of SARS-CoV-2 spike antibody.[13] In another contribution, Fathi-Hafshejani *et al.* reported a 2D-FET based on WSe_2 functionalised with mAbs against the SARS-CoV-2 spike protein, for the detection of the whole virus.[14] Finally, Li *et al.* presented an unamplified GFET aptasensor for the detection of SARS-CoV-2 RNA in human throat swab specimens.[15]

The use of ACE2 as efficient receptor has been demonstrated in several designs of biosensors. Among them, fluorescence "turn-on" sensors,[16] lateral flow colorimetric sensors,[17] low-cost biosensor comprised of pencil graphite electrodes,[18] and electrochemical impedance spectroscopy biosensors have been reported.[19] The design of sensors for SARS-CoV-2 employing ACE2 human receptors and gFETs has been proposed only theoretically;[20] no experimental proof of the plausibility and efficiency of this design has been reported to date.

In the present paper, we report the first example of GFET array biosensor using ACE2 as a receptor. Furthermore, we propose a rational approach to design, functionalise and characterise GFET biosensors, maximising the sensitivity of the device. By following this approach, we have been able to obtain a biosensor for the detection of SARS-CoV-2 spike protein with a limit of detection (LOD) of 2.94 ± 1.84 aM (1.23 ± 0.77 fg mL^{-1}). This astonishing value is among the lowest ever recorded for the detection of proteins with GFET devices.[8]

Alejandro Criado

Dr Alejandro Criado received his Ph.D. in Organic Chemistry (2013) at the University of Santiago de Compostela (Spain). From 2013 to 2020, he conducted postdoctoral research at the University of Trieste and CICbiomaGUNE research center. In 2021, he started his independent research career as Distinguished Researcher at CICA – Interdisciplinary Center of Chemistry and Biology, Universidade da Coruña, co-leading NanoSelf group. Currently, he is a Ramon y Cajal Assistant Professor at Chemistry Department at Universidade da Coruña. His research interests focus on the new methods for modifying low-dimensional materials to tailor their properties, along with the development of graphene-based sensors.

Results and discussion

The biosensor was designed using the microtransistor array GFET-S20 produced from Graphenea. This GFET array is composed by 12 CVD graphene (CVD-G) devices, with Al_2O_3 encapsulation on the metal pads to avoid degradation and to reduce current leakage It also comprises a non-encapsulated electrode, which allows liquid gating without the need of an external reference electrode (Fig. 1A and B). The biosensor operated as a solution-gated transistor in which the electrical double layer formed by the ions of the electrolyte act as a gate. To introduce the receptors, CVD-G was functionalised first with 1-pyrenebutyric acid *N*-hydroxy succinimide ester (PBASE), then ACE2 was covalently linked through amidation coupling (Fig. 1C).

Optimisation of graphene functionalisation

The first step to achieve a highly sensitive GFET array biosensor is to optimise the graphene chemical functionalisation.

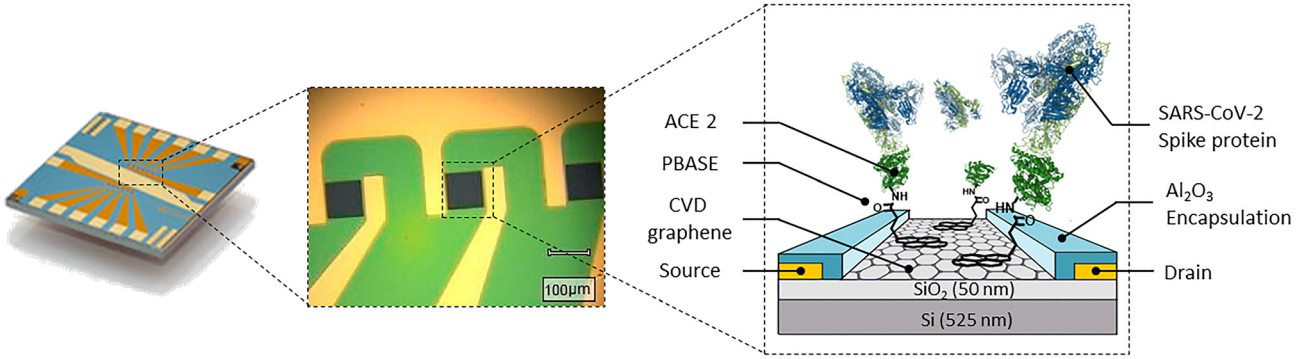

Fig. 1 Design of the GFET array biosensor.

With this aim, CVD-G deposited on Si/SiO_2 chips of 1×1 cm^2 were employed, as they allow an easier characterisation of the material, while being less expensive than GFET arrays. In first instance, the optimal PBASE concentration in EtOH was determined to be 1 mM. With this concentration, a uniform PBASE functionalisation over CVD-G was achieved. The morphology of the graphene surface was monitored by AFM (Fig. 2). By comparing the height micrographs before and after PBASE functionalisation (Fig. 2A and C), it is possible to appreciate a reduction in the average roughness of the surface. This demonstrates that, when the adsorption of PBASE on CVD-G is controlled, a flatter surface is formed as a result of a uniform and dense packing of the pyrene core on the graphene basal plane.[21] An increase in the surface roughness after PBASE functionalisation, frequently reported in previous works,[2,22] is instead symptomatic of PBASE aggregation on the surface and, therefore, non-efficient functionalisation. By comparing the lock-in phase micrographs (Fig. 2B and D), a total change in the surface morphology can be observed confirming the effective functionalisation of graphene.

Other useful techniques to evaluate the efficiency of the functionalisation are Raman spectroscopy and X-ray photoelectron spectroscopy (XPS). PBASE is adsorbed on graphene due to π–π interactions between the pyrene rings and the graphene lattice. This interaction induces a doping of graphene, which in Raman spectroscopy is reflected in a shift of approximately 7 cm^{-1} of the G band (Fig. 3A).[2,23] Moreover, after PBASE functionalisation, the G band exhibits a shoulder at 1628 cm^{-1}, which is attributed to pyrene group resonance, proving that PBASE is adsorbed onto the graphene surface.[21–23] Finally, an increase in the I_{2D}/I_G ratio after functionalisation has been observed as reported in previous works (Fig. S1†).[2,21,22] PBASE adsorption on graphene can be further monitored by observing the N 1s core level at XPS, which increases from 0.45 to 0.75 at% upon functionalisation (Fig. 3B). Furthermore, in the C 1s core level an increased contributions of the C–N component at 285.9 eV are appreciable (Fig. S2†). To prove the robust and reproducible functionalisation of graphene, three substrates were incubated with PBASE in the optimal conditions. Three parameters, namely average

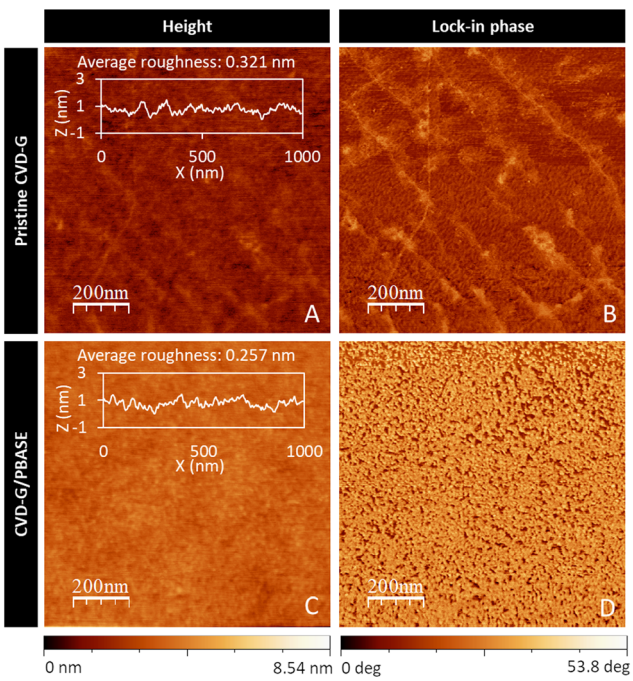

Fig. 2 AFM height (A and C) and lock-in phase (B and D) micrographs of pristine CVD-G (A and B) and CVD-G/PBASE (C and D).

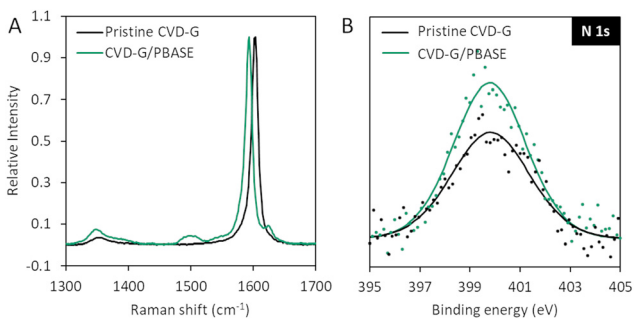

Fig. 3 (A) Raman spectra of pristine CVD-G (black) and CVD-G/PBASE (green). (B) High resolution XPS spectra of N 1s core of pristine CVD-G (black) and CVD-G/PBASE (green).

roughness (by AFM), G band Raman shift, and N content (by XPS), were monitored to determine the successful functionalisation of CVD-G. The consistent variation of these three parameters in different CVD-G batches proves the reproducibility of the functionalisation (Fig. S3†).

In the next step, the *N*-hydroxy succinimide ester of PBASE, exposed on the surface, was employed to perform an amidic coupling with the amino groups of the ACE2 protein. After anchoring the receptor, the graphene surface was characterised again by AFM and XPS. After the protein immobilisation, a significative increment in the average roughness is observed, passing from 0.257 nm to 0.499 nm (Fig. S4A†). In lock-in phase micrographs, it is possible to distinguish the globular shape of proteins covering uniformly the graphene surface in a tightly packed way (Fig. S4B†).

By XPS analysis, the high-resolution N 1s core level shows a significant intensity increase (from 0.74 to 5.81 at%) after ACE2 immobilisation (Fig. 4A). Furthermore, in C 1s core level the contributions of C–O/C–N (285.9 eV), C═O (287.14 eV) and O–C═O (289.00 eV) components increase, due to the large number of amine and amide groups present on the protein (Fig. S2†).

When performed on GFET arrays, the reaction outcome can also be monitored through the electrical characterisation of the device. After the functionalisation with ACE2, a positive shift of the GFET transfer curve is observed as result of p-doping of the graphene layer (Fig. 4B). This experimental evidence agrees with the expected result, since ACE2 has an isoelectric point ranging from 3.5 to 7;[24] therefore, it is a slightly anionic protein at pH 7.4 bound to the graphene surface.[9]

The result of the functionalisation procedure has been also monitored by electrochemical impedance spectroscopy (EIS), performed on a CVD-G film deposited on an ITO electrode. (Fig. S6†). At each step of the functionalisation, the resistance of the graphene electrode increases, attesting the formation of insulating layers over the 2D material and therefore its effective functionalisation.

Quartz Cristal Microbalance (QCM) was used to quantify the degree of functionalisation of graphene. This is a fundamental information in the design of the biosensor, as the number of receptors immobilised on the surface determines the sensitivity and limits of detection of a biosensor. To perform QCM experiments a monolayer of CVD-G was transferred over a commercial QCM crystal. In a first experiment, the graphene coated crystal was functionalised applying a stream of PBASE 1 mM in EtOH, followed by a stream of pure ethanol to wash away the non-adsorbed molecules. The variation of the frequency upon functionalisation is of 17.97 Hz (Fig. 5A), corresponding to a functionalisation density of 1.62 molecules per nm^2. This value is in good agreement with the expected molecular density for a monolayer of PBASE (3.81 molecules per nm^2), confirming the formation of a single layer of functionalisation (details regarding the functionalisation density calculations are reported in ESI†). In a second experiment, a stream of ACE2 in PBS was flown over the CVD-G QCM crystal functionalised with PBASE. The variation of the frequency upon ACE2 immobilisation is of 10.51 Hz (Fig. 5B), corresponding to a density of 0.0043 receptors per nm^2. We calculate the ACE2 footprint (79.76 nm^2) from its hydrodynamic radius and derived the expected molecular density for a monolayer of ACE2, equal to 0.012 proteins per nm^2. This, together with the AFM images (Fig. S4†), clearly proves that we have a tightly packed layer of receptors, uniformly coating the graphene surface.

Thickness of the functionalisation layer

When working with electrolyte gated GFETs, it is key to consider the charge screening induced by mobile ions in the medium.[8,25–27] According to the Debye–Hückel model, charged molecules are screened by counter-ions in solution, and their electric potential is reduced exponentially with distance, with a decay constant λ_D called the Debye length. Therefore, charges located farther than the Debye length are usually considered out of range for electrostatic detection by a FET sensor.[25] For this reason, the distance between target binding events and the FET surface needs to be analysed.

To measure the thickness of our functionalisation layer, we performed AFM shaving experiments after each functionalisation step. The thickness of each layer has been defined as the

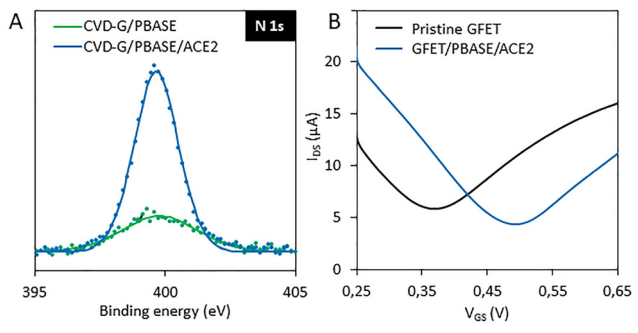

Fig. 4 (A) High resolution XPS spectra of N 1s core of CVD-G/PBASE (green) and CVD-G/PBASE/ACE2 (blue). (B) Transfer curves of pristine GFET (black) and GFET/PBASE/ACE2 (blue).

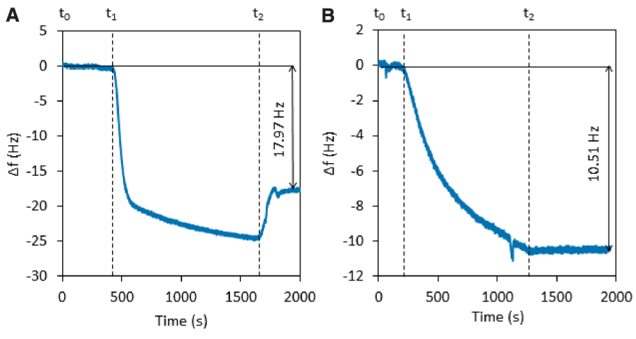

Fig. 5 (A) Frequency shift of the QCM during the functionalisation of CVD-G with PBASE. t_0 = EtOH, t_1 = PBASE 1 mM in EtOH, t_2 = EtOH. (B) Frequency shift of the QCM during the immobilisation of ACE2 onto CVD-G/PBASE. t_0 = PBS, t_1 = ACE2 10 μg ml^{-1} in PBS, t_2 = PBS.

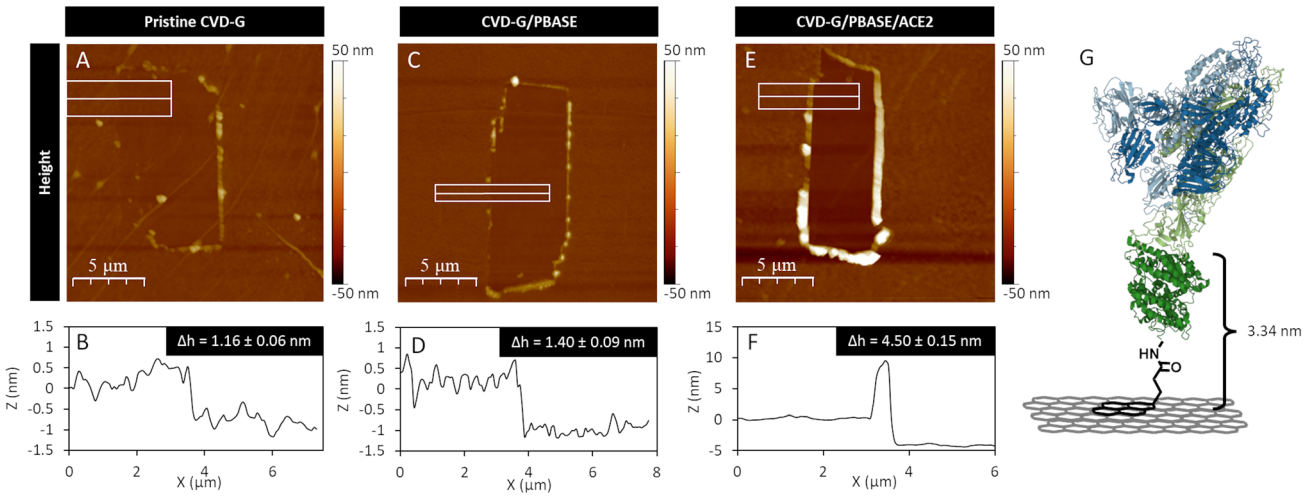

Fig. 6 AFM shaving experiment and average step heigh for pristine CVD-G (A and B), CVD.G/PBASE (C and D), and CVD.G/PBASE/ACE2 (E and F). (G) Distance between the graphene layer and the ACE2-spike protein recognition event.

difference in height between the shaved and non-shaved regions (Fig. 6). First, pristine graphene was shaved from the Si/SiO_2 substrate (Fig. 6A and B), measuring a thickness of (1.16 ± 0.06) nm for this layer. After functionalisation with PBASE, the total thickness raised to (1.40 ± 0.09) nm (Fig. 6C and D). By subtracting the thickness of the graphene layer, we obtain an approximate thickness of the PBASE layer equal to 0.24 nm, as expected for a molecular monolayer. Furthermore, from the AFM images it is possible to appreciate the uniformity and the extension of the monolayer functionalisation. After the immobilisation of the receptor, the overall thickness increases to (4.50 ± 0.15) nm (Fig. 6E and F). Therefore, the thickness of the ACE2 layer is equal to 3.10 nm. From these experiments, we can determine that the distance between the graphene layer and the ACE2-spike protein recognition event will be 3.4 nm (Fig. 6G). This information will be essential to select the optimal condition to perform sensing with the designed GFET. In addition, if we assume 3.4 nm as the optimal Debye length of our system, an estimation of the charge doping produced by ACE2 (Δn) can be calculated considering the electric-double-layer-gated transistor as a planar capacitor. Thus, Δn is defined by eqn (1):

$$\Delta n = \frac{A \times e}{\lambda_D} \times \Delta V_{CNP} = C \times \Delta V_{CNP} \quad (1)$$

where C is capacitance; ΔV_{CNP} is the V_{CNP} shift after the bioconjugation of ACE2 on graphene (0.12 V); A is the area of the semiconducting channel (8100 μm^2); $e = e_{PBS} \times e_0$, where e_{PBS} is the relative permittivity constant of the electrolyte solution of PBS (78.7), and e_0 is the vacuum permittivity (8.854×10^{-12} F m^{-1}); and λ_D is the Debye length (3.4 nm calculated by AFM). By substituting the corresponding values, the Δn obtained is equal to 1.99×10^{-10}, *i.e.*, 2.46×10^{-17} C nm^{-2}. In addition, if we consider the charge density of ACE2 obtained by theoretical calculations (44.86×10^{-19} Coulombs, Fig. S5†), a density of 0.0055 receptors per nm^2 can be estimated. It is worth noting that this value matches the receptor density determined by QCM precisely (0.0043 receptors per nm^2).

Optimisation of electrolyte ionic strength

The use of high salinity environments creates increased screening of charges, which can make detection by GFETs more challenging.[25,28] Instead, lower salinity enables longer electrical screening distances, allowing the detection further from graphene. To maximise the sensitivity and limits of detection of our biosensors, we calculated the optimal ionic force of the sensing electrolyte to match the thickness of the functionalisation layer, measured by AFM shaving. The Debye length in an electrolyte is typically described by the eqn (2):

$$\lambda_D = \sqrt{\frac{\varepsilon_r \varepsilon_0 k_B T}{2e^2 I}} \quad (2)$$

where I is the ionic strength of the electrolyte, ε_0 is the permittivity of free space, ε_r is the dielectric constant, k_B is the Boltzmann constant, T is the temperature, and e is the elementary charge.

For an aqueous solution at room temperature, it can be expressed by eqn (3):

$$\lambda_D = \frac{0.304\ (\mathrm{mol}^{1/2}\,\mathrm{nm}^{-1/2})}{\sqrt{I(M)}} \quad (3)$$

By substituting the λ_D with the functionalisation layer thickness (3.4 nm), we have been able to calculate the optimal ionic strength for our device (8 mM). Therefore, a salt solution composed of 2.32 mM of Na_2HPO_4, 1.68 mM of NaH_2PO_4 and 4 mM of KCl (at pH 7) was selected as sensing electrolyte for all the following experiments.

Interaction between ACE2 functionalised graphene and SARS-CoV-2 spike ectodomain

To confirm the preservation of ACE2 activity after the immobilization onto the graphene surface, its interaction with SARS-CoV-2 spike ectodomain (Ecto S) was studied by means of different techniques. To demonstrate the selectivity of the interaction, bovine serum albumin (BSA) was used as a negative control, because this protein is not expected to have any specific interaction with ACE2. In addition, BSA is an abundant protein in human fluids and is therefore important for the analysis of biological samples using this type of device.

In a first experiment, we radiolabelled Ecto S and BSA with ^{125}I and incubated the radioactive proteins with ACE2 modified CVD-G. After washing away the non-bonded proteins, the radioactivity of the surface was measured. The percentage of radioactivity registered after the incubation with the Ecto S is significantly higher when compared to the surface incubated with BSA, which shows very low radioactivity levels (Fig. 7A). This data confirms the affinity of the functionalised surface for Ecto S and the selectivity of the interaction.

As done previously, to prove the functionalisation of graphene, EIS was registered before and after incubation with Ecto S. The resistance increases from 41.1 kΩ to 56.3 kΩ, confirming the interaction among the two proteins (Fig. 7B). Finally, the functionalised surface was mapped by AFM before and after incubating with BSA and Ecto S. Thus, it is possible to visualise the spike protein adsorbed on the surface as 4–10 nm events after the incubation with Ecto S (Fig. S7 and 8†).[13] By counting, it is possible to obtain the approximative number of recognition events per surface unit (Fig. S7†). Once again, BSA was used as a control and no significative change in the surface roughness was detected after incubation.

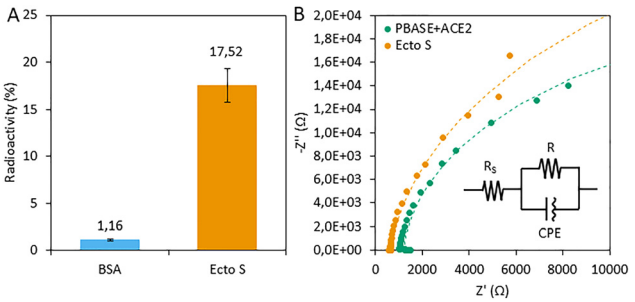

Fig. 7 (A) Radiolabelling experiment evaluating the affinity between CVD-G/PBASE/ACE2 surface and BSA and Ecto S. (B) EIS of an ITO-CVD-G/PBASE/ACE2 electrode before (blue, R = 41.1 kΩ) and after (orange, R = 56.3 kΩ) Ecto S incubation.

Detection of SARS-CoV-2 Ecto S with GFET array biosensor

To read out the GFET arrays a Graphenea Cartridge S2X was used as interface between the graphene microdevice and the electrical equipment (Keithley 2200). This cartridge is comprised of a reservoir that allows for *in situ* measurements with liquids. The electrical metric monitored during sensing was the shift of the transfer curve, while the analytical parameter evaluated was the potential of the charge neutrality point

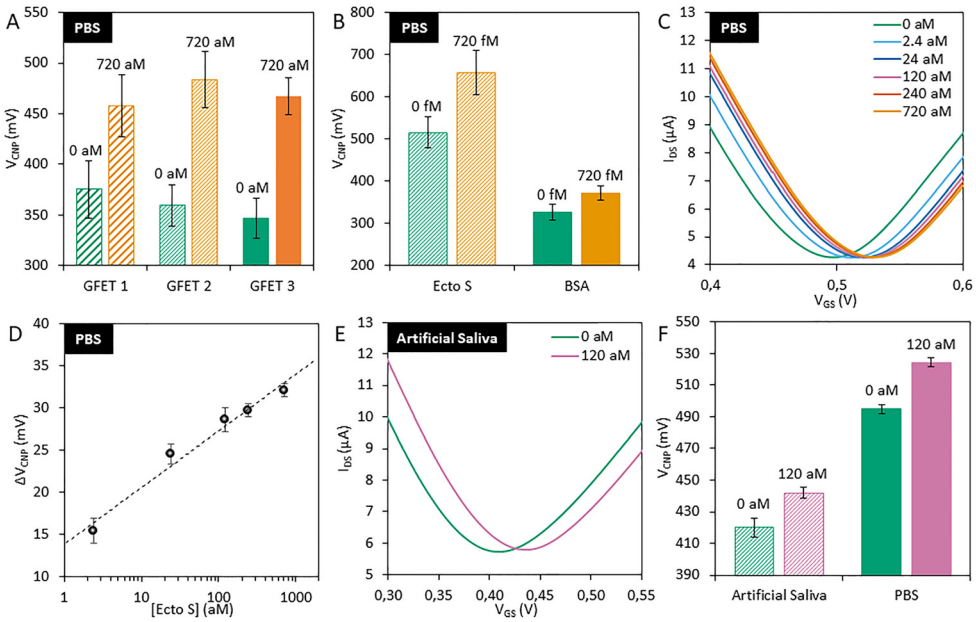

Fig. 8 (A) Variation of the CNP potential for GFETs/PBASE/ACE2 in absence and in presence of 720 aM of Ecto S, on 3 independent GFET arrays containing each one 12 transistors. (B) Variation of the CNP potential for GFETs/PBASE/ACE2 evaluated in absence and in presence of 720 fM of Ecto S and BSA. (C) Ecto S dose dependent shift of the transfer curve for GFETs/PBASE/ACE2. (D) Calibration line obtained by plotting the variation of the CNP potential at different Ecto S concentration for GFETs/PBASE/ACE2. (E) GFETs/PBASE/ACE2 transfer curves in absence and in presence of 120 aM of Ecto S in artificial saliva. (F) Variation of the CNP potential for GFETs/PBASE/ACE2 in absence and in presence of 120 aM of Ecto S in PBS and artificial saliva (Error bars are the standard deviation among the transistors comprised in each GFET).

(CNP). The response of the ACE2 functionalised GFET was evaluated in the absence and presence (720 aM) of Ecto S, on three independent GFET arrays containing each one 12 microtransistors (Fig. 8A). The variation of the CNP potential (ΔV_{CNP}) was measured *a posteriori* (30 min after incubation). All the three GFET arrays showed a significative ΔV_{CNP} in the presence of Ecto S, demonstrating the reproducibility among the GFETs and the microtransistors comprising each GFET (Fig. S9A†).

The selectivity of the device was studied by using BSA as a negative control. The analytical devices were incubated with Ecto S and BSA, and transfer curves were registered before and after the incubation. The ΔV_{CNP} registered in the device incubated with BSA is significative lower if compared to the shift induced by Ecto S, even at elevated concentrations (720 fM, Fig. 8B and Fig. S9B†). Furthermore, by analysing the transfer curves after BSA and Ecto S incubation, it is possible to discern two distinct behaviours, suggesting different interaction mechanisms for these proteins. While Ecto S induces an actual shift in CNP voltage due to the biorecognition (Fig. S10A†), BSA alters the transconductance of electrons in the device (the slope of the right branch of the transfer curve, Fig. S10B†). This behaviour could be explained with a non-specific interaction of BSA with the surface, which introduces additional scattering sites, increasing therefore the disorder of the functionalisation layer.[8]

Once demonstrated the consistent and selective response of the biosensors, titration at different concentrations of Ecto S was performed (Fig. 8C). The shift of the CNP potential (ΔV_{CNP}) shows a logarithmic dependency with respect to Ecto S concentration. This relation can be explained by the Langmuir isotherm, which describes the absorption of a molecule over a surface,[29] and it is frequently reported for GFETs in which the sensing mechanism involves an adsorption/desorption step.[8,30] The ΔV_{CNP} is linearly dependent from the logarithm of the concentration in the range from 2.4 to 720 aM (Fig. 8D). Due to the logarithmic dependence the sensor shows a higher sensitivity in the lower range of detection allowing to detect highly diluted concentrations of analyte. The noise of the sensor (σ) has been calculated as the standard deviation of the GFET's CNP in absence of the analyte. The LOD was calculated by extrapolating 3σ from the linear fit obtained from the biosensor titration. The LOD for the biosensor is of 2.94 ± 1.84 aM (calculated as average among three GFETs), that is among the lowest LOD reported for GFETs for the detection of proteins.[8] Although a GFET design based on ACE2 was theoretically studied in terms of detection parameters,[20] the comparison of our experimental results with theory remains difficult since the authors made part of their calculations using a completely different immobilization strategy using lipids.

The ability of the GFET array biosensor to detect Ecto S has been tested in a complex matrix: artificial saliva. The saliva was diluted 1 : 100, resembling the protocols used for pharyngeal swab tests, to reduce the ionic force of the matrix to the optimal value for sensing. In Fig. 8E the transfer curves of the GFET array in presence and absence of 120 aM of Ecto S in diluted saliva are reported (which would be equal to 1 virus per μL if one viral particle contains 100 surface spike proteins).[30,31] The ΔV_{CNP} registered in artificial saliva is comparable to the one in PBS confirming the applicability of the biosensor in complex environments (Fig. 8F).

Finally, the results obtained with the GFET were validated by comparison with surface plasmon resonance (SPR), which is a state-of-the-art technique to evaluate protein–protein interaction. To perform SPR experiments graphene, deposited on a gold substrate, was functionalised analogously to the GFETs (PBASE + ACE2). The interaction of the functionalised surface with the Ecto S and with BSA was studied as a function of the protein concentrations (Fig. 9). SPR shows a selective response toward Ecto S, and practically no interaction with BSA. The LOD calculated from SPR experiment is equal to 5 aM, while the linear range is contained between 2.4 and 240 aM (Fig. S11†). These parameters, analogous to the ones obtained with GFET, confirm the extraordinary sensitivity, selectivity and limits of detections observed with the ACE2 receptors.

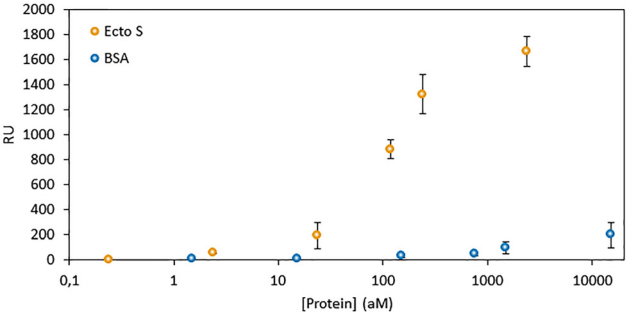

Fig. 9 Calibration lines obtained by SPR at different Ecto S and BSA concentrations for CVD-G/PBASE/ACE2.

Table 1 Comparison with the limits of detection (LOD) for SARS-CoV-2 spike protein of G-FET biosensors published up to date

FET	Receptor	LOD	Ref.
G-FET	mAb	1 fg mL^{-1}	2
WSe_2-FET	mAb	25 fg mL^{-1}	14
G-FET	Aptamer	3 fM	30
G-FET	ACE2	1.23 ± 0.77 fg mL^{-1} 2.94 ± 1.84 aM[a]	This work

[a] LOD is expressed as the average among three GFETs with the relative standard deviation

Conclusion

Herein, we developed a GFET analytical device for the detection of SARS-CoV-2 Ecto S spike protein using ACE2 as a receptor. We have applied a rational approach that allowed us to reach an ultralow LOD, which is lower,[14,30] or comparable[2] to other 2D-FETs that used antibodies or aptamers as receptors (Table 1).

In terms of design, each manufacturing step has been well-characterised. For the chemical modification of graphene, the anchoring strategy of ACE2 was confirmed by AFM, electronic characterisation based on CNP, XPS, Raman spectroscopy, AFM and QCM. Then, the recognition event of Ecto S through the interaction with ACE2 immobilised on graphene was deeply analysed by SPR, radiolabelling, AFM, and ESI.† Thus, we have proved that recognition event required binding to the ACE2 receptor. Finally, the Ecto S detection was achieved in PBS with ultra-low LOD of 2.94 ± 1.84 aM. Besides, the sensing device exhibited detection capability of Ecto S in a realistic medium.

Further work is in progress to detect real viruses by using different Human cell receptors. This manuscript paves the way to a new generation of GFET sensors with high applicability. Such devices can be used to detect a plethora of viruses, to quantify their copies, and evaluate their infectivity. In addition, this proof-of-concept device is an alternative to widely applied biosensors based on antibodies. In particular, the latter require constant update to follow the appearance of new variants of the virus. By contrast, human receptors evolve at such a low speed that the design of our platform stays valid for a very long time.

Experimental

Materials and reagents

GFET-S20 array and CVD-G on Si/SiO_2 were produced and provided from Graphenea Semiconductor SLU. PBASE, ACE2, mucin, Na_2HPO_4, NaH_2PO_4, $NaHCO_3$, KCl, NaCl, $CaCl_2$ and EtOH were purchased from Sigma Aldrich. Ecto S of SARS-CoV-2 was purchased from CIC bioGUNE. PBASE and ACE2 were stored at −20 °C, while Ecto S at 80 °C. The Ecto S (BEI construct NR-52394) was expressed by transient transfection of HEK293F suspension cells and purified from clarified cell supernatants seven days post-transfection using a nickel affinity column and size-exclusion chromatography as previously described.[32] Then, the Ecto S and previously purified ligand according to Barnes *et al.*, 2020 were mixed and incubated 2 hours at 4 °C.

Apparatus and measurements

CVD-G and GFET-S20 array were characterized by atomic force microscopy (AFM), X-ray photoelectron spectroscopy (XPS), Raman spectroscopy, and electrical measurements. AFM micrographs were registered using Bruker Multimode 8 microscope, employing a tapping mode tip with the frequency of 320 Hz (Bruker TESPA-V2). Shaving experiment were performed in Contact mode scanning several times an area of 10 μm × 4 μm and applying a force of ≈70 nN at a scan rate of 2 Hz. The probe used was the ScanAsyst-Air silicon tip (Bruker).

The shaved area was characterised again in PeakForce QNM mode with a scan angle of 90° to avoid artifacts do to piled material. AFM images were processed using WSvM5.0 and Nanoscope Analysis 2.0 software. XPS measurements were performed in a SPECS Sage HR 100 spectrometer using a non-monochromatic X-ray source of Mg with a Ka line of 1253.6 eV. An electron flood gun was used to avoid sample charging. XPS data fitting was performed using Casa XPS software (Version 2.3.16 PR 1.6). Raman spectra were recorded using a Renishaw Invia Raman spectrometer (l_{ex} = 532 nm). Each spectrum is the average of at least 300 spectra recorded in different spots of the sample with 1 s of integration time at a laser power of 1.29 mW. Data were processed using Ranishaw WiRE 4 software. Electrical measurements on GFETs were performed using a source meter Keithley 2612B and a Graphenea Cartridge S2X. A drain–source bias voltage of 20 mV was maintained during measurements, and gate voltage window was 0–1 V with a voltage sweep of ≈5 mV s^{-1}.

Functionalisation of CVD-G

CVD-G and GFET-S20 array were functionalised incubating the graphene surface with 1 mM solution of PBASE in EtOH for 2 h at RT. After that, the graphene surface was rinsed twice in EtOH and twice in H_2O. CVD-G/PBASE was incubated with ACE2 (0.5 mg ml^{-1}) in PBS 0.1 M at pH 7.4 for 30 min at RT. After functionalisation, the graphene surface was rinsed twice in PBS and once in H_2O. The functionalised graphene can be stored at 4 °C immersed in PBS solution up to two days after functionalisation.

Radiolabelling of proteins with iodine-125

10 μL of Ecto S solution (or BSA) (1 mg mL^{-1}, 10 mM PBS pH 7.4) and 35 μL of [^{125}I] NaI (approximately 50 μCi) were incubated at room temperature for 20 min in an Eppendorf containing iodogen reagent (20 μg), 45 μL of NaH_2PO_4 and Na_2HPO_4 buffer (0.5 M and 0.15 M, respectively, pH 7.4). After incubation, the reaction mixture was purified by size exclusion chromatography using Illustra™ Nap™-5 Sephadex™ columns G-25 DNA grade (GE Healthcare, USA), preconditioned with PBS (10 mL, 10 mM pH 7.4). The fractions containing pure labelled protein were collected, measured in a dose calibrator, and analyzed with radio-thin layer chromatography (radio-TLC) using iTLC-SG chromatography paper (Agilent Technologies, CA, USA) and 85% EtOH as the stationary and mobile phases, respectively. Before running the TLC, iodine was reduced using $Na_2S_2O_3$ (16 mg in 1 mL of H_2O, 45 μL per 15 μL of sample) solution. TLC plates were analyzed using MUCHA detector (Raytest). The collected fractions (~500 μL) were diluted at a final volume of 1.4 mL. Ecto S was radiolabeled with a conversion efficiency of 17.6% and a radiochemistry yield of 2.45 μCi (5%). BSA was radiolabeled with a conversion efficiency of 50.5% and a radiochemistry yield of 7.15 μCi (14.3%).

100 μL of [^{125}I] Ecto S (5.6 μg mL^{-1}) or [125I] BSA (5.6 μg mL^{-1}) were deposited on CVD-G/PBASE/ACE2 on Si/SiO_2 substrates and incubated at RT for 20 minutes. The supernatant was removed and the unabsorbed [^{125}I] Ecto S (or BSA) was washed with 1 mL of PBS (10 mM, pH 7.4) and 1 mL of MilliQ water. For each replicate (triplicates), the unabsorbed proteins

in the supernatants and absorbed protein on CVD-G/PBASE/ACE2 were quantified using MUCHA detector (0–56 keV) to determine the relative amount of radioactivity. The data is expressed as the percent ratio between the radioactivity in the supernatant and the residual radioactivity on the substrate.

Electrochemical impedance spectroscopy

Three-electrode electrochemical cell was used to perform the impedance characterisation of the graphene functionalisation. A CVD-G monolayer, deposited on top if a glass ITO electrode (1 cm^2) by a wet transfer process, was used as a working electrode. A Pt wire and Ag/AgCl were used as counter and reference electrodes. EIS was measured after each step of the functionalisation and after the incubation of the substrate with Ecto S. Measurements were conducted in 0.1 M PBS in presence of 5 mM potassium hexacyanoferrate(III) with an Potentiostat Autolab Metrohm Station 302N (PGSTAT302N, Metrohm). EIS was registered in a frequency range among 10 kHz and 0.01 Hz, with a voltage amplitude of 0.1 V and integration time of 0.3 s. The data were fitted with an equivalent circuit using Nova 2.1 software.

QCM-D measurements

The graphene functionalisation degree was determined by means of QCM-D technique (Q-Sense E4). CVD graphene was transferred onto commercial crystals QSensor QSX 303 SiO_2 (Qsense). 1 mM PBASE in EtOH solution was flown on the functionalised crystal with the help of a peristaltic pump until the frequency was stabilised. Before and after deposition, EtOH was rinsed during 5–10 min until the signal was stable. For the functionalisation with ACE2 (10 μg ml^{-1}) the same procedure was carried out after PBASE deposition. In this case, PBS was employed as a solvent instead of ethanol. All the experiments were performed at 25 °C.

Assessment analytical performance of the GFET sensors for EctoS

Two days after the GFET functionalisation, electrical measurements were performed a diluted PBS solution (2.32 mM of Na_2HPO_4, 1.68 mM of NaH_2PO_4 and 4 mM of KCl at pH 7). Source–drain voltage was fixed at 20 mV and the electrolyte gate was swept from 0 to 1 V. The response of the GFETs in absence and presence of Ecto S spike protein was evaluated registering the curves before and after the incubation with the analyte (30 min) at different concentrations, namely 0, 2.4, 24, 120, 240, 720 aM. For the investigation of selectivity, the same protocol was applied with BSA. Artificial saliva was prepared as previously reported:[33] 4 mg mL^{-1} of urea, 4 mg mL^{-1} of mucin from porcine stomach, 0.6 mg mL^{-1} of Na_2HPO_4, 0.3 mg mL^{-1} of $NaHCO_3$, 0.6 mg mL^{-1} of $CaCl_2$, 0.4 mg mL^{-1} of KCl, and 0.4 mg mL^{-1} of NaCl in Milli-Q water. Artificial saliva was used to evaluate the performances of the G-FET in realistic media as it was done with PBS.

Surface plasmon resonance

The interaction of CVD-G/PBASE/ACE2 with Ecto S was evaluated by surface plasmon resonance using an Affinité Instruments P4SPR. CVD-G transferred by a semi-dry process over Au/Ti SPR prisms has been functionalised as described above. Ecto S solution in 0.1 M PBS at different concentrations (1, 10, 100, 1000 fg ml^{-1}; correspond to 2.4 aM–2.4 fM) was flown over SPR prism with a flow rate of 30 μl min^{-1}. Analogously BSA was flown over the interface in the same concentration levels (1, 10, 100, 1000 fg ml^{-1}; correspond to 1.5 aM–15 fM).

Author contributions

Alessandro Silvestri: conceptualisation, investigation, methodology, formal analysis and writing – original draft. Julian Zayas: investigation, methodology, formal analysis and writing – review & editing. Mariano Vera-Hidalgo: investigation, validation and writing – review & editing. Desiré di Silvio: investigation, methodology and writing – review & editing. Cecilia Wetzl: investigation, methodology and writing – review & editing. Marta Martinez-Moro: investigation and writing – review & editing. Amaia Zurutuza: supervision, project administration, funding acquisition and writing – review & editing. Elias Torres: investigation, methodology and writing – review & editing. Alba Centeno: supervision, project administration and writing – review & editing Arantxa Maestre: investigation, methodology and writing – review & editing. Juan Manuel Gómez: sample manufacture and investigation. María Arrastua: sample manufacture and validation. Nerea Ontoso: sample manufacture and validation. Marta Elicegui: sample manufacture and investigation. Maurizio Prato: supervision, project administration, funding acquisition and writing – review & editing. Ivan Coluzza: conceptualisation, supervision, project administration, funding acquisition and writing – review & editing. Alejandro Criado: conceptualisation, methodology, supervision, project administration, funding acquisition and writing – review & editing.

Conflicts of interest

There are no conflicts to declare.

Acknowledgements

This project was funded by the Fommento Donostia-San Sebastián, through Talentu Berritzailea/Talento Innovador 2020 (No. 0577/2020/0051), and the Program for Technology Transfer 2021 (0632/2021/0002). M. P. as recipient of the AXA Chair, is grateful to AXA Chair in Nanobiotechnology supported by the AXA Research Fund. A. S. thanks Spanish Ministry of Science and Innovation (MCIN) for his research grant FJC2018-036777-I. A.C. thanks Xunta de Galicia and

MCIN for his research grants Atracción de Talento (No. ED431H 2020/17) and Ramón y Cajal (No. RYC2020-030183-I), respectively. The authors thank S. Szunerits for performing SPR measurements on a portable P4 SPR platform from Affinité Instruments, Canada. Part of this work was performed under the Maria de Maeztu Units of Excellence Program grant MDM-2017-0720 funded by MCIN/AEI/10.13039/501100011033.

References

1 G. Liu and J. F. Rusling, *ACS Sens.*, 2021, **6**, 593–612.
2 G. Seo, G. Lee, M. J. Kim, S.-H. Baek, M. Choi, K. B. Ku, C.-S. Lee, S. Jun, D. Park, H. G. Kim, S.-J. Kim, J.-O. Lee, B. T. Kim, E. C. Park and S. Il Kim, *ACS Nano*, 2020, **14**, 5135–5142.
3 A. K. Srivastava, N. Dwivedi, C. Dhand, R. Khan, N. Sathish, M. K. Gupta, R. Kumar and S. Kumar, *Mater. Today Chem.*, 2020, **18**, 100385.
4 C. Peng, Z. Zhu, Y. Shi, X. Wang, K. Mu, Y. Yang, X. Zhang, Z. Xu and W. Zhu, *J. Phys. Chem. Lett.*, 2020, **11**, 10482–10488.
5 P. Zhao, J. L. Praissman, O. C. Grant, Y. Cai, T. Xiao, K. E. Rosenbalm, K. Aoki, B. P. Kellman, R. Bridger, D. H. Barouch, M. A. Brindley, N. E. Lewis, M. Tiemeyer, B. Chen, R. J. Woods and L. Wells, *Cell Host Microbe*, 2020, **28**, 586–601.e6.
6 P. D. Skottrup, M. Nicolaisen and A. F. Justesen, *Biosens. Bioelectron.*, 2008, **24**, 339–348.
7 B. Byrne, E. Stack, N. Gilmartin and R. O'Kennedy, *Sensors*, 2009, **9**, 4407–4445.
8 A. Béraud, M. Sauvage, C. M. Bazán, M. Tie, A. Bencherif and D. Bouilly, *Analyst*, 2021, **146**, 403–428.
9 W. Fu, L. Jiang, E. P. van Geest, L. M. C. Lima and G. F. Schneider, *Adv. Mater.*, 2017, **29**, 1603610.
10 J. Sengupta and C. M. Hussain, *Carbon Trends*, 2021, **2**, 100011.
11 D. Kong, X. Wang, C. Gu, M. Guo, Y. Wang, Z. Ai, S. Zhang, Y. Chen, W. Liu, Y. Wu, C. Dai, Q. Guo, D. Qu, Z. Zhu, Y. Xie, Y. Liu and D. Wei, *J. Am. Chem. Soc.*, 2021, **143**, 17004–17014.
12 I. Park, J. Lim, S. You, M. T. Hwang, J. Kwon, K. Koprowski, S. Kim, J. Heredia, S. A. Stewart de Ramirez, E. Valera and R. Bashir, *ACS Sens.*, 2021, **6**, 4461–4470.
13 H. Kang, X. Wang, M. Guo, C. Dai, R. Chen, L. Yang, Y. Wu, T. Ying, Z. Zhu, D. Wei, Y. Liu and D. Wei, *Nano Lett.*, 2021, **21**, 7897–7904.
14 P. Fathi-Hafshejani, N. Azam, L. Wang, M. A. Kuroda, M. C. Hamilton, S. Hasim and M. Mahjouri-Samani, *ACS Nano*, 2021, **15**, 11461–11469.
15 J. Li, D. Wu, Y. Yu, T. Li, K. Li, M. M. Xiao, Y. Li, Z. Y. Zhang and G. J. Zhang, *Biosens. Bioelectron.*, 2021, **183**, 113206.
16 R. L. Pinals, F. Ledesma, D. Yang, N. Navarro, S. Jeong, J. E. Pak, L. Kuo, Y.-C. Chuang, Y.-W. Cheng, H.-Y. Sun and M. P. Landry, *Nano Lett.*, 2021, **21**, 2272–2280.
17 J. H. Lee, Y. Lee, S. K. Lee, J. Kim, C. S. Lee, N. H. Kim and H. G. Kim, *Biosens. Bioelectron.*, 2022, **203**, 114034.
18 L. F. de Lima, A. L. Ferreira, M. D. T. Torres, W. R. de Araujo and C. de la Fuente-Nunez, *Proc. Natl. Acad. Sci. U. S. A.*, 2021, **118**, 1–9.
19 V. J. Vezza, A. Butterworth, P. Lasserre, E. O. Blair, A. MacDonald, S. Hannah, C. Rinaldi, P. A. Hoskisson, A. C. Ward, A. Longmuir, S. Setford, E. C. W. Farmer, M. E. Murphy and D. K. Corrigan, *Chem. Commun.*, 2021, **57**, 3704–3707.
20 A. Toral-Lopez, D. B. Kokh, E. G. Marin, R. C. Wade and A. Godoy, *Nanoscale Adv.*, 2022, **4**, 3065–3072.
21 Y. Liu, L. Yuan, M. Yang, Y. Zheng, L. Li, L. Gao, N. Nerngchamnong, C. T. Nai, C. S. Suchand Sangeeth, Y. P. Feng, C. A. Nijhuis and K. P. Loh, *Nat. Commun.*, 2014, **5**, 1–8.
22 L. Xu, S. Ramadan, O. E. Akingbade, Y. Zhang, S. Alodan, N. Graham, K. A. Zimmerman, E. Torres, A. Heslegrave, P. K. Petrov, H. Zetterberg, D. J. Sharp, N. Klein and B. Li, *ACS Sens.*, 2022, **7**, 253–262.
23 G. Wu, X. Tang, M. Meyyappan and K. W. C. Lai, *Appl. Surf. Sci.*, 2017, **425**, 713–721.
24 C. Scheller, F. Krebs, R. Minkner, I. Astner, M. Gil-Moles and H. Wätzig, *Electrophoresis*, 2020, **41**, 1137–1151.
25 T. Rodrigues, V. Mishyn, Y. R. Leroux, L. Butruille, E. Woitrain, A. Barras, P. Aspermair, H. Happy, C. Kleber, R. Boukherroub, D. Montaigne, W. Knoll and S. Szunerits, *Nano Today*, 2022, **43**, 101391.
26 E. Stern, R. Wagner, F. J. Sigworth, R. Breaker, T. M. Fahmy and M. A. Reed, *Nano Lett.*, 2007, **7**, 3405–3409.
27 S. Sorgenfrei, C. Chiu, M. Johnston, C. Nuckolls and K. L. Shepard, *Nano Lett.*, 2011, **11**, 3739–3743.
28 A. Vacic, J. M. Criscione, N. K. Rajan, E. Stern, T. M. Fahmy and M. A. Reed, *J. Am. Chem. Soc.*, 2011, **133**, 13886–13889.
29 N. Gao, T. Gao, X. Yang, X. Dai, W. Zhou, A. Zhang and C. M. Lieber, *Proc. Natl. Acad. Sci. U. S. A.*, 2016, **113**, 14633–14638.
30 L. Xu, S. Ramadan, B. G. Rosa, Y. Zhang, T. Yin, E. Torres, O. Shaforost, A. Panagiotopoulos, B. Li, G. Kerherve, D. K. Kim, C. Mattevi, L. Jiao, P. Petrov and N. Klein, *Sens. Diagn.*, 2022, **1**, 719–730.
31 Y. M. Bar-On, A. Flamholz, R. Phillips and R. Milo, *eLife*, 2020, **9**, e57309.
32 C. O. Barnes, A. P. West, K. E. Huey-Tubman, M. A. G. Hoffmann, N. G. Sharaf, P. R. Hoffman, N. Koranda, H. B. Gristick, C. Gaebler, F. Muecksch, J. C. C. Lorenzi, S. Finkin, T. Hägglöf, A. Hurley, K. G. Millard, Y. Weisblum, F. Schmidt, T. Hatziioannou, P. D. Bieniasz, M. Caskey, D. F. Robbiani, M. C. Nussenzweig and P. J. Bjorkman, *Cell*, 2020, **182**, 828–842.e16.
33 L. Barhoumi, A. Baraket, F. G. Bellagambi, G. S. Karanasiou, M. B. Ali, D. I. Fotiadis, J. Bausells, N. Zine, M. Sigaud and A. Errachid, *Sens. Actuators, B*, 2018, **266**, 477–484.